Check for updates

Detection and Characterization of VIM-52, a New Variant of VIM-1 from a *Klebsiella pneumoniae* Clinical Isolate

Marie de Barsy,[a] Paola Sandra Mercuri,[b] Saoussen Oueslati,[c,d,e] Eddy Elisée,[f] Te-Din Huang,[a] Pierre Sacré,[a] Bogdan I. Iorga,[f] Thierry Naas,[c,d,e] Moreno Galleni,[b] Pierre Bogaerts[a]

[a]Laboratory of Bacteriology, CHU UCL Namur, Université Catholique de Louvain, Yvoir, Belgium
[b]InBios-Laboratoire de Macromolécules Biologiques, Centre d'Ingénierie des Protéines, Université de Liège, Liège, Belgium
[c]Team ReSIST, INSERM U1184, School of Medicine Université Paris-Saclay, LabEx LERMIT, Le Kremlin-Bicêtre, France
[d]Bacteriology-Hygiene unit and French National Reference Center for Antibiotic Resistance: Carbapenemase-producing Enterobacteriaceae, Assistance Publique/ Hôpitaux de Paris, Bicêtre Hospital, Le Kremlin-Bicêtre, France
[e]Evolution and Ecology of Resistance to Antibiotics Unit, Institut Pasteur—APHP-Université Paris-Sud, Paris, France
[f]Université Paris-Saclay, CNRS, Institut de Chimie des Substances Naturelles, Gif-sur-Yvette, France

ABSTRACT Over the last two decades, antimicrobial resistance has become a global health problem. In Gram-negative bacteria, metallo-β-lactamases (MBLs), which inactivate virtually all β-lactams, increasingly contribute to this phenomenon. The aim of this study is to characterize VIM-52, a His224Arg variant of VIM-1, identified in a *Klebsiella pneumoniae* clinical isolate. VIM-52 conferred lower MICs to cefepime and ceftazidime compared to VIM-1. These results were confirmed by steady-state kinetic measurements, where VIM-52 yielded a lower activity toward ceftazidime and cefepime but not against carbapenems. Residue 224 is part of the L10 loop (residues 221 to 241), which borders the active site. As Arg 224 and Ser 228 both play an important and interrelated role in enzymatic activity, stability, and substrate specificity for the MBLs, targeted mutagenesis at both positions was performed and further confirmed their crucial role for substrate specificity.

KEYWORDS antibiotic resistance, metallo-β-lactamase, *Klebsiella pneumoniae*, biochemical characterization, carbapenemase, MBL, metalloenzymes

Multidrug-resistance in Gram-negative bacteria represents a major public health problem (1). The emergence and spread of acquired carbapenemases such as metallo-β-lactamases (MBLs) are of particular concern (2). MBLs were first reported in 1966, and were not initially considered a serious threat for antimicrobial chemotherapy, as they were mostly chromosomally encoded in nonpathogenic bacteria (3). The situation is now different, as the genes encoding MBLs are frequently located on mobile genetic structures, facilitating dissemination and spread among clinically relevant Gram-negative bacteria (4, 5). The MBLs are divided into three subclasses, B1, B2, and B3. The most important acquired MBLs are members of subclass B1, including Verona integron-encoded metallo-β-lactamase (VIM) (6) and New Delhi metallo-β-lactamase (NDM) (7). Bla$_{VIM-1}$ was first identified as a chromosomally encoded within a class I integron in a *Pseudomonas aeruginosa* clinical isolate (6). Today, VIM-1-like enzymes are mostly identified in multidrug-resistant *Enterobacterales* species (4, 5). The VIM enzyme family currently includes 73 different variants (http://www.bldb.eu/) (8) divided into 5 different clusters of closely sequence-related enzymes, namely, VIM-1 and VIM-2 (the 2 major clusters) and then VIM-7, VIM-12, and VIM-13 variants (9). Similar to other MBLs, VIM enzymes hydrolyze all β-lactams with the exception of monobactams. Their fold forms an $\alpha\beta\beta\alpha$ sandwich and their active site is located in a central groove on one edge of the two β sheets. The active site is able to bind two zinc ions, positioned,

respectively, in the tetrahedral Zn1 site (formed by the conserved H116, 118, and 196) and the Zn2 site, which includes D120, C221, and H263 (BBL numbering scheme) (10–14). Amino acids at position 224 and 228 are part of the L10 loop (residues 221 to 241) located near the active site. Compared to the other subclass B1 MBLs (NDM-1 and IMP-1), which harbor a positively charged lysine at position 224, VIM enzymes all display amino acids at position 224 which abolish the presence of a positive charge near the active site (histidine for VIM-1 variants, tyrosine for VIM-2 variants, but leucine 224 for VIM-26 and VIM-28). This affects the interaction of VIM enzymes with the conserved carboxylic function of the β-lactam compounds and its intrinsic stability (15, 16). The presence of an arginine at position 228 can structurally replace the function of the Lys 224 (17), but most of the variants containing an Arg 228, such as VIM-4, display a lower hydrolysis efficiency against expanded-spectrum cephalosporins. Within the VIM-1 sub-group, the presence of a serine at position 228 increases the accessibility of the active site and its activity toward substrates with bulky side chains in C3-like the third and/or fourth generation cephalosporins. We report here the characterization of a VIM-52-pro-ducing *K. pneumoniae* clinical isolate (*Kp*_20150593) and the kinetic parameters of the purified VIM-52 protein. VIM-52 differed from VIM-1 by a single histidine-to-arginine substitution at position 224. Due to the importance of the residue at positions 224 and 228, we generated different mutants of VIM-1 (H224A, H224D, and H224K) and VIM-52 (S228A, S228D, S228K, and S228R) to explore their influence on the structure of the L10 loop, the active site, and the VIM substrate specificity. The rationale behind these choices was to replace the existing amino acids by a small neutral amino acid (alanine), a positively charged amino acid (lysine), and a negatively charged amino acid (aspartate). In addition, for VIM-52, we further replaced the S228 (a polar amino acid) by the positively charged R in order to explore the effect of the potential steric and charge hindrance of the 2 arginines at positions 224 and 228. Three dimensional modeling and molecular dynamics simulation were also performed.

RESULTS

VIM-52, a single amino acid variant of VIM-1: clinical context and molecular identification. A 67-year-old Belgian patient developed a severe acute respiratory dis-tress episode during a holiday stay in Greece and was hospitalized in a local intensive care unit (ICU), requiring intubation and mechanical ventilation. Three days later, he was repatriated to the ICU of a general hospital in Belgium, where microbiological sam-ples collected from several anatomical sites (sputum, rectal swab, and urine) cultured a carbapenem-resistant *K. pneumoniae* isolate (*Kp*_20150593). The isolate displayed high-level resistance to penicillins, third-generation cephalosporins and carbapenems, but remained susceptible to cefepime and to aztreonam (Table 1).

In-house multiplex PCR confirmed the presence of a *bla*VIM gene and subsequent Sanger sequencing revealed a *bla*VIM-52 allele, a novel single amino acid variant H224R of VIM-1 (Fig. 1A).

Whole-genome sequencing (WGS) of the VIM-52-producing *Kp*_20150593 isolate revealed that *Kp*_20150593 belonged to the sequence type (ST) 147 and capsular type was KL64. VIM-1-producing *K. pneumoniae* ST147 isolates have been reported previ-ously in several hospitals in Greece (18), and *K. pneumoniae* ST147 is considered as an emerging high-risk clone harboring different carbapenemases and responsible for hos-pital outbreaks all over Europe (19, 20). To the best of our knowledge, no other case of a VIM-52-producing isolate has been reported.

The *bla*VIM-52 gene is located on a 5,884-bp contig presenting a BLAST best hit (query cover 100%, E value 0.0, percentage identity 99.97%) with a region of the plasmid pIncRIncN from *K. pneumoniae* strain 1_GR_13 (CP027047.1), which harbors a *bla*VIM-27 gene (data not shown). The *bla*VIM-52 gene is embedded in a class I integron together with two additional gene cassettes conferring resistance to aminoglycoside, (*aac(6')-I* and *aph(3'')-Ia*, and one to trimethoprim, *dfrA1* (Fig. 1B). The *bla*VIM-52 gene cassette is inserted at the first position of the variable region of the integron, immediately down-stream to the integron-borne strong promoter Pc (Fig. 1B).

TABLE 1 MIC (μg/ml) values evaluated by broth microdilution of *K. pneumoniae* 20150593 and of its *E. coli* transformant and transconjugant

Antibiotic(s)	*K. pneumoniae* 20150593	*E. coli* TOP10	*E. coli* TOP10 p20150593	*E. coli* J53	*E. coli* J53 p20150593
Temocillin	>128	16	>128	16	>128
Ticarcillin	>512	8	>512	8	>512
Ticarcillin/clavulanic acid[a]	>256	8	>256	4	>256
Piperacillin-tazobactam[b]	>256	2	>256	2	256
Cefepime	2	<0.12	0.25	<0.12	0.5
Cefotaxime	>128	<0.12	>128	0.25	128
Ceftazidime	64	0.5	64	1	32
Ceftazidime-avibactam[c]	>32	0.25	32	0.25	8
Ceftolozane-tazobactam[b]	>32	0.5	>32	0.5	>32
Ertapenem	16	<0.06	2	<0.06	1
Imipenem	32	0.25	4	0.5	2
Meropenem	16	<0.06	2	<0.06	1
Aztreonam	0.25	<0.12	0.5	<0.12	0.5
Gentamicin	1	<0.5	1	<0.5	2
Tobramycin	8	<0.5	8	<0.5	16
Amikacin	16	<1	16	4	16
Ciprofloxacin	>16	<0.06	<0.06	<0.06	<0.06
Fosfomycin	64	<4	<4	<4	<4
Tigecycline	0.5	0.25	0.12	0.25	0.25
Colistin	>64	0.5	0.5	1	1

[a]Clavulanic acid used at 2 μg/ml.
[b]Tazobactam used at 4 μg/ml.
[c]Avibactam used at 4 μg/ml.

An ~50-kb plasmid was extracted from *Kp*_20150593 by the Kieser method. This plasmid was electroporated to *Escherichia coli* strain Top10 and a mating-out experiment using J53 azide-resistant *E. coli* as the recipient strain confirmed that pIncRIncN-VIM-52 is a self-conjugative plasmid. The transconjugant and the transformant displayed a similar antimicrobial resistance profile, which was different from the parental *Kp*_20150593 isolate (Table 1), indicating that resistance to ciprofloxacin, colistin, and fosfomycin are not related to the VIM-52 plasmid. The mechanisms of resistance to these antibiotics will not be investigated in the present study.

Site-directed mutagenesis of H224 and S228 amino acids in VIM-1 and VIM-52, respectively. The MICs of *E. coli* producing VIM-1 and variants against different beta-lactam antibiotics (Fig. 2) were determined by broth microdilution (Table 2). Compared to VIM-1, the natural H224R substitution in VIM-52 conferred a very similar resistance profile to carbapenems and most β-lactams (no more than 1 dilution difference, Table 2). Nevertheless, for ceftazidime, a difference of at least two dilutions was detected (>128 to 64 μg/ml for VIM-1 and VIM-52, respectively). For cefepime, a dramatic drop of MIC value was observed (from 64 to 0.25 μg/ml), suggesting an almost complete loss of cefepime hydrolysis by VIM-52.

In other VIM-1 variants at position 224, such as H224D, an increase in the susceptibility to ertapenem was observed (0.25 μg/ml instead of 1 μg/ml for VIM-1), while the mutation H224K increased the susceptibility to meropenem (1 μg/ml instead of 4 μg/ml for VIM-1). Nevertheless, the most dramatic effect was observed with cefepime (Table 2), for which the resistance profile ranged from 64 μg/ml for VIM-1 to 0.25 μg/ml for VIM-52 with a gradual increase of the susceptibility according to the nature of the mutation at position 224 (MIC of VIM-1 > H224A > H224D > H224K > H224R [VIM-52]).

Mutations performed on VIM-52 at position 228, such as S228A and S228K, had minor effects on MIC values, while S228R led to an additional decreased resistance to meropenem compared to VIM-52. On the contrary, S228D mutations restored a partial resistance phenotype to cefepime (2 μg/ml), while susceptibility to ertapenem was increased (0.25 μg/ml) (Table 2).

Four representative mutants (VIM-1 H224K; VIM-52 [H224R], VIM-52 S228D, and S228R) were further studied by molecular modeling and purified to homogeneity in order to determine their hydrolytic parameters.
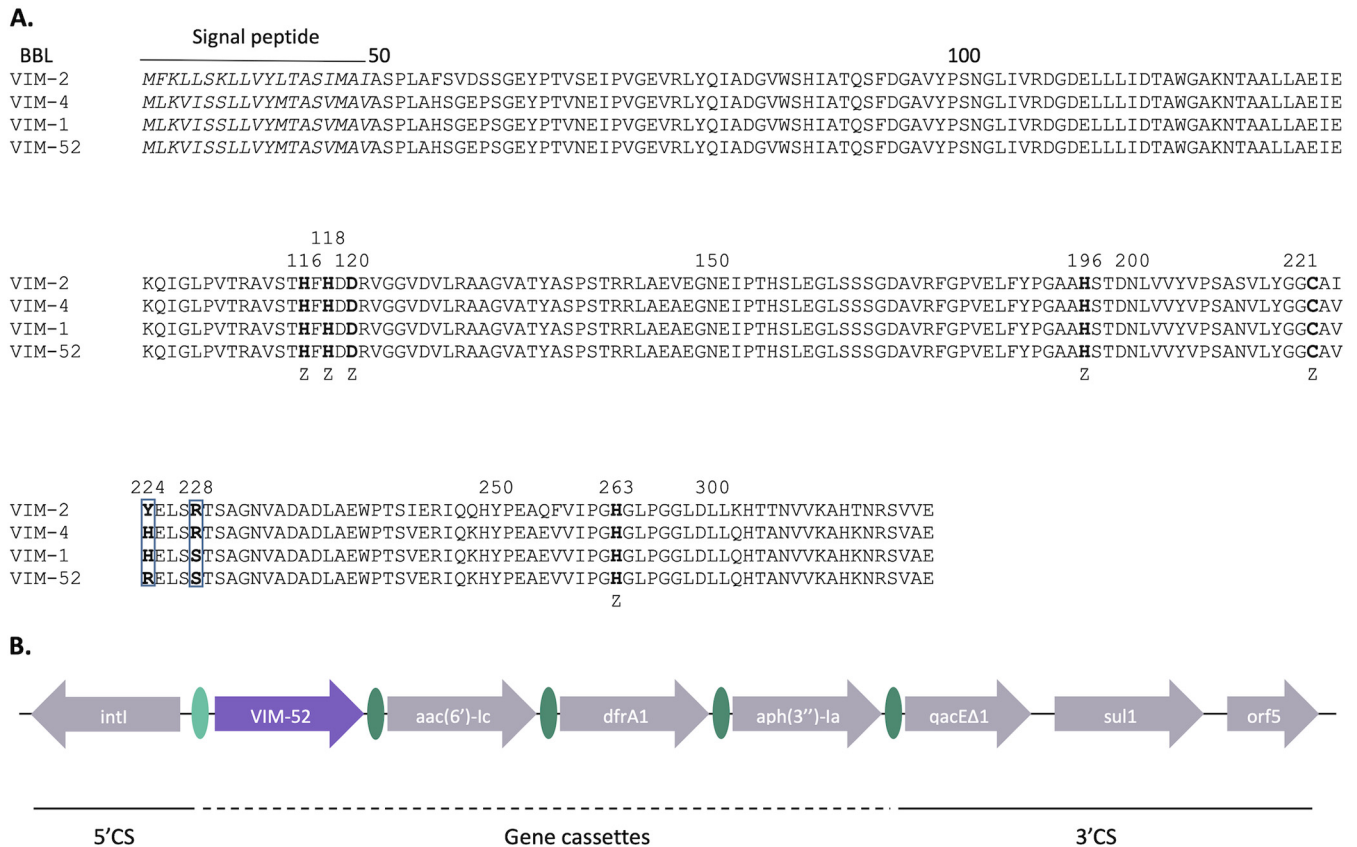
A.

B.

FIG 1 VIM-52 sequence analysis and bla_{VIM-52} locus characterization. (A) Multiple alignment of VIM-1 (UniProtKB Q5GN09), VIM-2 (UniProtKB Q9K2N0), VIM-4 (UniProtKB Q8KRJ3), and VIM-52 (this study). Amino acids positions are numbered according to the BBL scheme. Positions 224 and 228 are framed. "Z" indicates the residues interacting with Zn. (B) Class I integron annotation. The 5'CS includes *intl* gene, while the 3'CS includes the *qacEΔ1*, *sul1*, and *orf5* genes. The gene cassettes comprise the following genes: bla_{VIM-52} (in purple), *aac(6')-l*, *dfrA1*, and *aph(3'')-la*. Gene expression is under the control of a Pc strong (PcS) promoter and a P2 promoter. AttC and attL sites are depicted in green and in light green, respectively.

Structural analysis of the VIM variants. A three-dimensional model was constructed for each of these VIM variants, starting from the crystal structure of VIM-1 (PDB code 5N5I) (16), then submitted to molecular dynamics (MD) simulations, which very quickly reached an equilibrium, with root-mean-square deviation (RMSD) values of about 1 Å that were conserved throughout (Fig. S1 in the supplemental material). Each mutant features a specific conformation of loop L10 (residues 221 to 241) (Fig. S2) and a specific shape for the binding site (Fig. 3). The hydrogen bond interactions that are controlling the conformation of loop L10 are presented in Fig. 4. The hydrogen bonds between the side chain of T275 and the backbone of the residues in position 224, as well as between the side chain of H274 and the backbone of the residue in position 228, are present in all six VIM variants studied, with the exception of K224/S228 (Fig. 4b), where H274 is absent. Additional hydrogen bonds were observed in these mutants, all of them constituting essential elements to define the conformation of the L10 loop (Fig. 4).

Steady-state kinetic analysis. Table 3 shows that VIM-52 displayed higher catalytic efficiencies (k_{cat}/K_m) toward benzylpenicillin and cefotaxime compared to VIM-1, but lower toward ceftazidime and cefepime and similar toward imipenem and meropenem. Also, k_{cat} values for meropenem and ertapenem (0.3 s^{-1}) were lower than the k_{cat} for imipenem (2.2 s^{-1}). This suggests that the active site of VIM-52, because of the presence of the large positively charged R224, is less able to interact with bulky and/or positively charged C3 substrates (Fig. 2). Indeed, cephalothin and cefotaxime, which possess the same small, uncharged C3 acetoxymethyl group substituent, are hydrolyzed with the same efficiency (Table 3), despite that cefotaxime possesses a larger C7-lateral chain
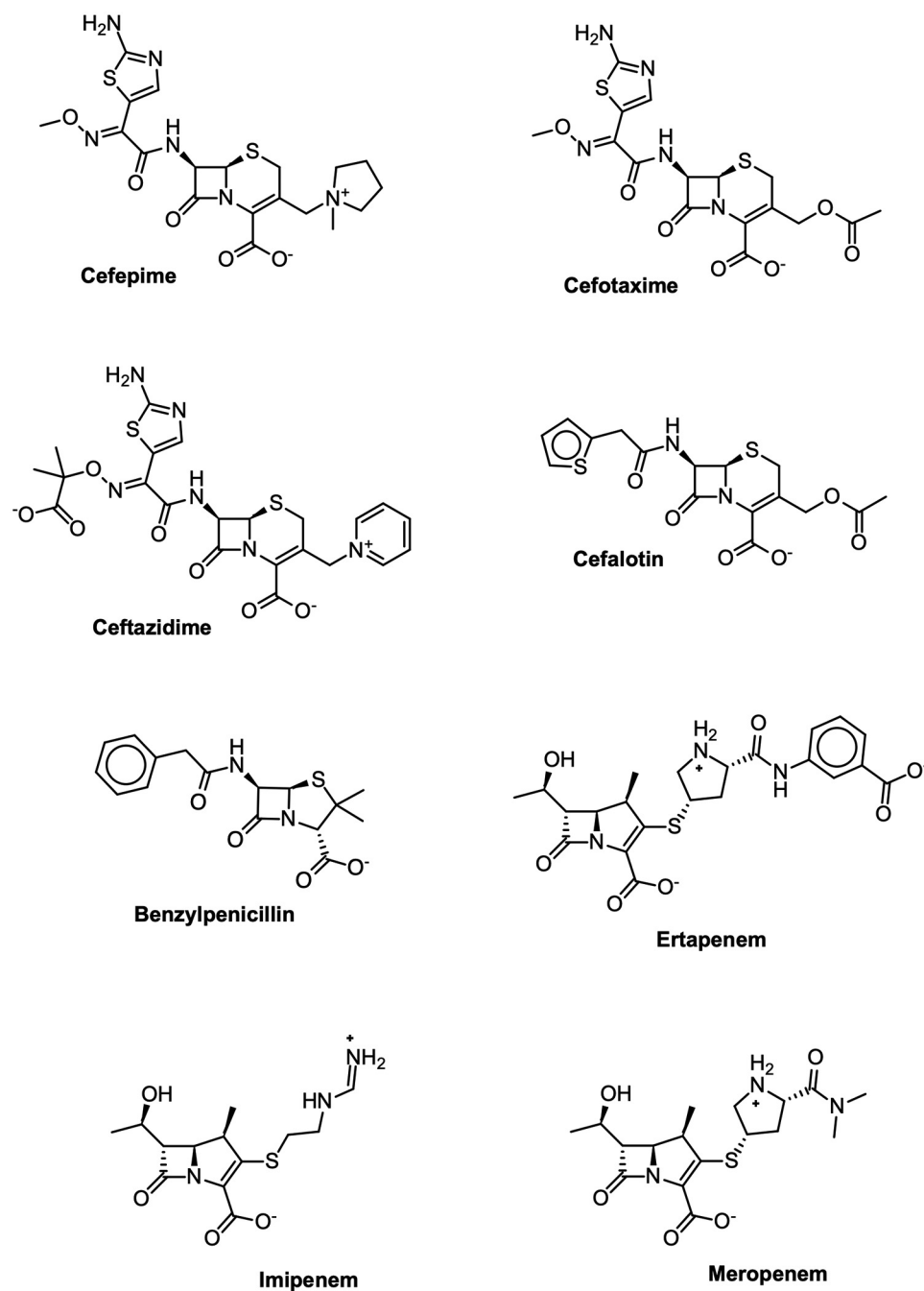
FIG 2 Chemical structures of the β-lactam antibiotics used in this study.

(2-[2-amino-1,3-thiazol-4-yl]-2-[methoxyimino] acetyl) amino group instead of the 2-thie-nylacetyl nitrilo group for cephalothin. Interestingly, the only structural difference between cefepime and cefotaxime is the presence of a bulky and positively charged C3 lateral chain (1-methylpyrrolidinium-1-methyl group) in cefepime, instead of the small acetoxymethyl group for cefotaxime (Fig. 2). The presence of this group results in a reduced affinity (increase in K_m value) for cefepime compared to cefotaxime and thus a large reduction of the VIM-52 catalytic efficiency. The same observation can be made with ceftazidime, which also presents a bulky and positively charged C3 substituent (N-methyl-pyridinium group). For these β-lactams, we noted a more than 10-fold increase in the K_m values compared to cephalothin or cefotaxime. Therefore, we were not able to

TABLE 2 MIC (μg/ml) evaluated by broth microdilution of *E. coli* Top 10 pTOPO-VIM-1, pTOPO-VIM-52, and their respective mutants

MBLs pTOPO plasmid	Penicillins				Cephalosporins					Carbapenems			Monobactam
	PTZ[a]	TEM	TIC	TCC	FEP	CTX	CAZ	CZA	C/T	ERT	IMP	MER	ATM
No MBL	2	16	8	8	≤0.12	≤0.12	0.5	0.5	0.5	≤0.06	0.125	≤0.06	0.125
VIM-1	>256	>128	>512	>256	64	128	>128	>32	>32	1	8	4	0.25
VIM-1 H224A	>256	>128	>512	>256	**16**[b]	>128	>128	>32	>32	0.5	8	2	≤0.12
VIM-1 H224D	128	128	>512	>256	**8**	64	128	>32	>32	0.25	4	2	0.25
VIM-1 H224K	128	>128	>512	>256	**0.5**	64	128	>32	>32	1	4	1	0.25
VIM-52	>256	>128	>512	>256	**0.25**	128	64	32	>32	1	4	2	0.25
VIM-52 S228A	256	>128	>512	>256	0.25	128	32	32	>32	0.5	4	1	≤0.12
VIM-52 S228D	256	>128	>512	>256	**2**	64	128	>32	>32	0.25	4	1	0.25
VIM-52 S228K	256	>128	>512	>256	≤0.12	64	32	32	>32	1	4	1	≤0.12
VIM-52 S228R	128	>128	>512	>256	≤0.12	64	**16**	**8**	>32	1	4	0.5	0.25

[a]PTZ, piperacillin-tazobactam (4 μg/ml); TEM, temocilin; TIC, ticarcillin; TCC, ticarcillin-clavulanate; FEP, cefepime; CTX, cefotaxime; CAZ, ceftazidime; CZA, ceftazidime-avibactam; C/T, ceftolozane-tazobactam; ERT, ertapenem; IMP, imipenem; MER, meropenem; ATM, aztreonam.
[b]Important changes are highlighted in boldface type.

measure k_{cat} and K_m independently since, in our experimental conditions, their hydrolysis was characterized by a first-order kinetic. Molecular docking calculations of cefotaxime with the R224/S228 variant provided a possible explanation for these results, showing a binding mode with hydrogen bonds of the side chain of R224 with the carboxylate
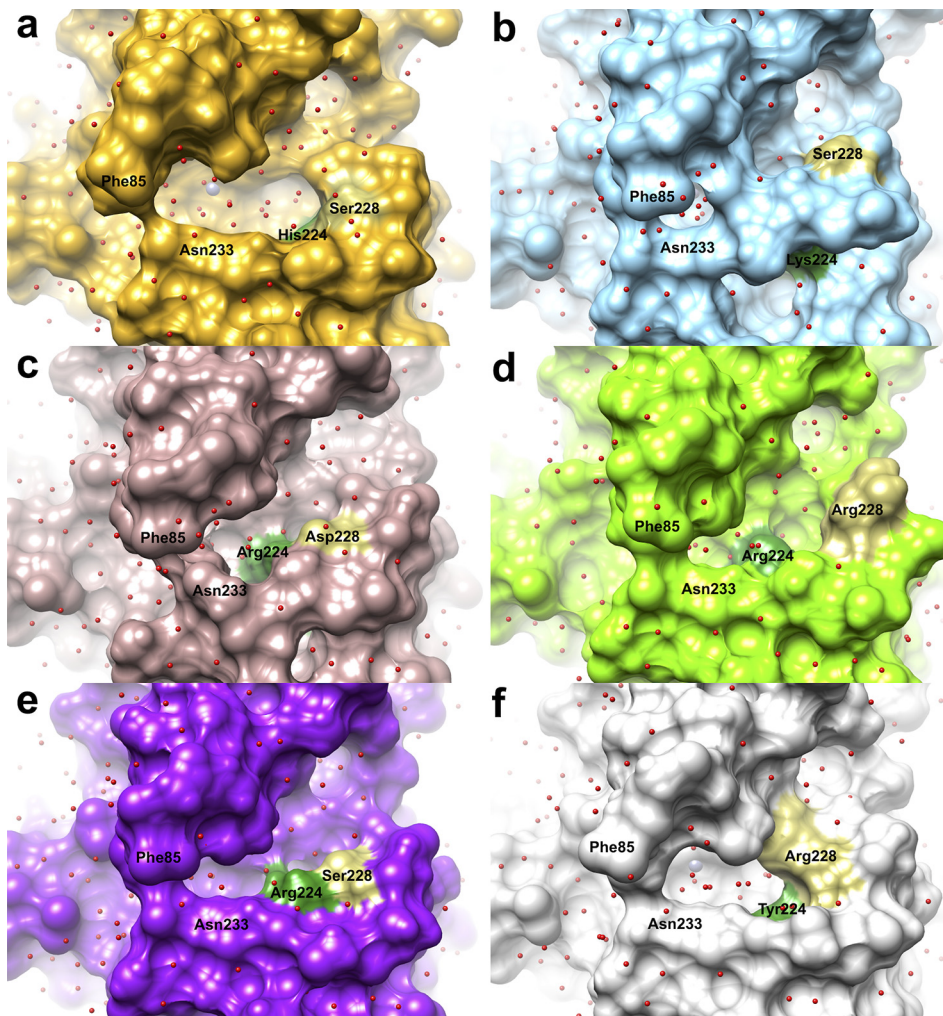

FIG 3 Binding site shape variability of the six VIM variants revealed by molecular dynamic simulations. The proteins are represented as surfaces colored in orange (a, H224/S228), cyan (b, K224/S228), brown (c, R224/D228), light green (d, R224/R228), purple (e, R224/S228), and gray (f, Y224/R228). The zinc ions and the stabilized water molecules predicted by HOP are represented as mauve and red spheres, respectively.
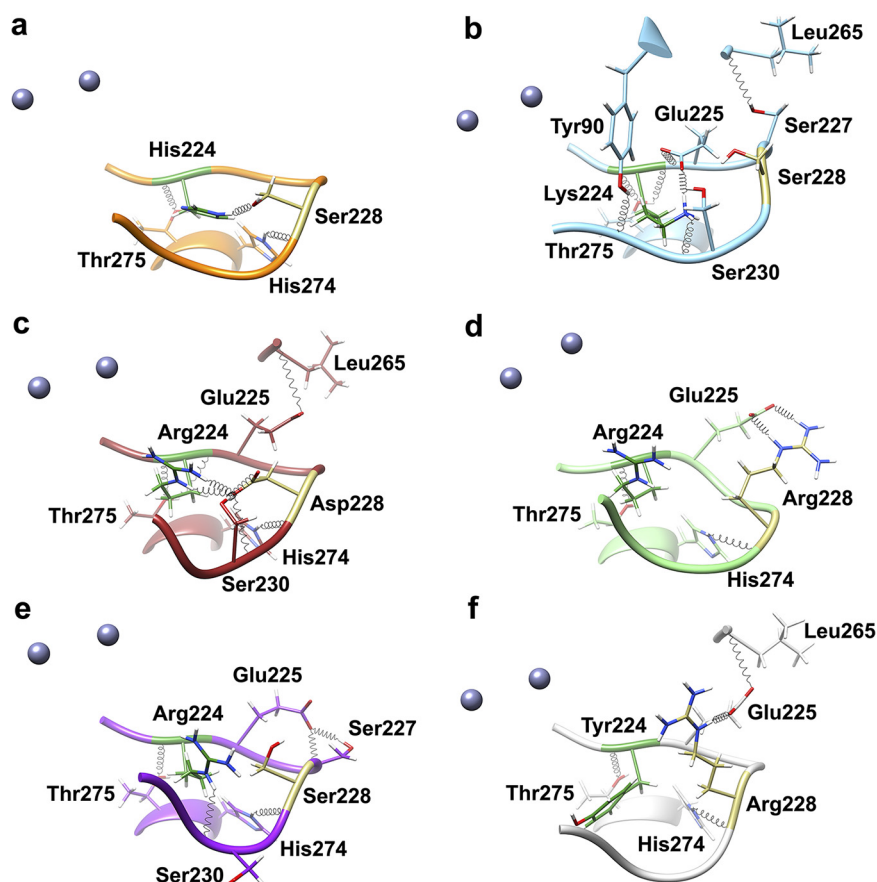
FIG 4 Stabilizing interactions in the loop 221 to 241 of the six VIM variants. The proteins are colored in orange (a, H224/S228), cyan (b, K224/S228), brown (c, R224/D228), light green (d, R224/R228), purple (e, R224/S228), and gray (f, Y224/R228). The zinc ions are represented as mauve spheres and the hydrogen bonds as black strings.

group and with the carbonyl oxygen of the ester group of cefotaxime (Fig. 5a). The binding modes of cefepime (Fig. 5b) or ceftazidime are slightly different due to repulsive interactions between the side chain of R224 and the positively charged substituents in position C3, thus explaining the higher K_m values determined experimentally for these two molecules. With its small and neutral substituent in C3, cephalothin remains a good substrate for both VIM-1 and VIM-52 MBLs.

VIM-52 and VIM-1 displayed a similar catalytic efficiency (k_{cat}/K_m) toward carbapenems. Nevertheless, k_{cat} and K_m for meropenem were strongly reduced compared to VIM-1. These results suggested different modes of interaction of meropenem with the active site residues. Molecular docking calculations on the R224/R228 variant showed strong hydrogen bonds between the carboxylate group of meropenem and the side chain of R224 in VIM-52, which are not possible with the shorter side chain of H224 in VIM-1 (Fig. 6a). A similar explanation was found for benzylpenicillin, which is a better substrate for VIM-52 (Fig. 6b). If we compare the enzyme activities toward third and fourth generation cephalosporins, we can note that cefotaxime was a better substrate for VIM-52 (k_{cat}/K_m for VIM-52 is 5 times higher). In contrast, VIM-52 was less active against cefepime and ceftazidime than VIM-1, with a ratio of k_{cat}/K_m for VIM-52 and VIM-1 of 0.026 and 0.15, respectively. These latter observations are in agreement with the MICs determined for *E. coli* TOP10 producing VIM-1 or VIM-52 (Table 2). This confirmed that the presence of an arginine in position 224 is less favorable to accommodate the positively charged C3-*N*-methyl pyrrolidine group of the cephems (Fig. 5). Furthermore, the H224K VIM-1 variant showed about 100-fold reduced activity toward

TABLE 3 Steady-state kinetic parameters for VIM-52, VIM-1H224K

Antibiotic	VIM-52 (R224)			VIM-1 (H224)[a]				VIM-1 H224K				VIM-2[b]			
	k_{cat} (s^{-1})	K_m (µM)	k_{cat}/K_m (µM^{-1} s^{-1})	k_{cat} (s^{-1})	K_m (µM)	k_{cat}/K_m (µM^{-1} s^{-1})	R1[c]	k_{cat} (s^{-1})	K_m (µM)	k_{cat}/K_m (µM^{-1} s^{-1})	R2[d]	k_{cat} (s^{-1})	K_m (µM)	k_{cat}/K_m (µM^{-1} s^{-1})	R3[e]
Benzylpenicillin	335 ± 30	130 ± 10	2.6 ± 1.1	29	841	0.034	**76**	230 ± 20	55 ± 5	4.2 ± 0.5	**123**	280	70	4	**120**
Cephalothin	170 ± 20	30 ± 6	5.6 ± 1.8	281	53	5.3	**1**	200 ± 10	25 ± 6	8 ± 2.3	**1.5**	130	11	11	**2**
Ceftazidime	>4.8	>400	0.012 ± 0.002	60	794	0.076	**0.15**	13 ± 2	340 ± 25	0.04 ± 0.01	**0.5**	3.6	72	0.05	**0.7**
Cefepime	>35	>350	0.1 ± 0.03	549	145	3.8	**0.026**	>12	>500	0.025 ± 0.005	**0.007**	>40	>400	0.1	**0.03**
Cefotaxime	120 ± 30	35 ± 5	3.4 ± 0.9	169	247	0.68	**5**	220 ± 30	40 ± 4	5.5 ± 1.3	**8**	70	12	5.8	**8.5**
Imipenem	2.2 ± 0.5	1.2 ± 0.3	1.8 ± 0.7	2	1.5	1.3	**1.4**	75 ± 15	7.5 ± 0.5	10 ± 2	**7.7**	34	9	3.8	**2.9**
Meropenem	0.3 ± 0.1	0.7 ± 0.2	0.45 ± 0.15	13	48	0.27	**1.7**	1.5 ± 0.1	0.2 ± 0.05	8 ± 0.5	**30**	5	2	2.5	**9.2**
Ertapenem	0.3 ± 0.05	0.5 ± 0.1	0.6 ± 0.2	ND	ND	ND	**ND**	1 ± 0.1	0.5 ± 0.1	2 ± 0.6	**ND**	0.2	9	0.02	**ND**

[a]Data are from Franceschini et al. (11).
[b]Data are from Docquier et al. (25).
[c]R1, ratio k_{cat}/K_m VIM-52 to k_{cat}/K_m VIM-1. Boldface type indicates ratio values; ND, not done.
[d]R2, ratio k_{cat}/K_m VIM-1H224K to k_{cat}/K_m VIM-1.
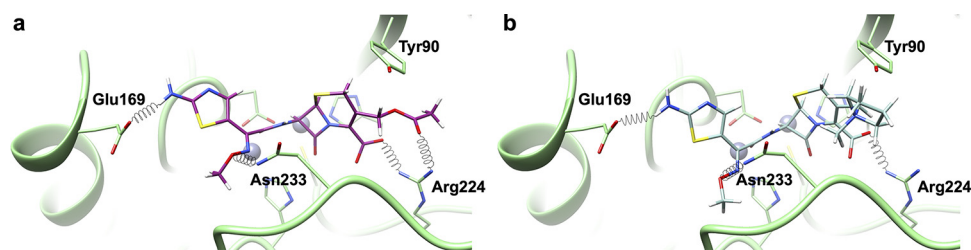[e]R3, ratio k_{cat}/K_m VIM-2 to k_{cat}/K_m VIM-1.

FIG 5 Molecular determinants for the selectivity of cefotaxime and cefepime on specific VIM variants. Docking complexes of cefotaxime (a, magenta) and cefepime (b, cyan) with the R224/S228 variant of VIM (colored in light green). The zinc ions are represented as mauve spheres and the hydrogen bonds as black strings.

cefepime (ratio of k_{cat}/K_m for the H224K VIM-1 variant versus VIM-1 was 0.007). Interestingly, the H224K VIM-1 mutant was more active against benzylpenicillin, cefotaxime, imipenem, and meropenem (ratios of 123, 8, 7.7, and 30, respectively) (Table 3). The presence of a lysine at position 224 enhances the catalytic efficiency toward carbapenems and benzylpenicillin but does not explain MICs against carbapenems (Table 2). This discrepancy might suggest a lower level of expression and/or stability of this mutant, which is supported by the Western blot experiments showing a lower signal for VIM-1 H224K mutant than for VIM-1 (Fig. S3). This experimental observation might explain why H224K has never been identified despite being more active against carbapenems than H224R (i.e., VIM-52).

We also explored the function of the amino acid 228 in VIM-52. Our data showed that the S228D VIM-52 mutant was more or equally efficient against all the tested substrates compared to the unmutated VIM-52 (Table 4; R4-VIM-52 ratio). This phenomenon was mainly due to the increase of the k_{cat} values. Interestingly, the catalytic efficiency of VIM-52 S228R against ceftazidime and cefepime dropped compared to VIM-52, mainly due to the lower k_{cat} of the mutant. On the other hand, activity against carbapenems of this mutant rose due to higher k_{cat} for imipenem (20 s^{-1} instead of 2.2 s^{-1} for VIM-52) and a decrease of K_m for meropenem (0.03 μM instead of 0.7 μM for VIM-52) and ertapenem (0.06 μM instead of 0.5 μM for VIM-52), with the k_{cat} remaining roughly unchanged (Table 4). The analysis of the enzymatic profile of the double R224 R228 mutant compared to VIM-1 showed a major drop in activity against ceftazidime and cefepime due to the decrease of the k_{cat} value and a higher catalytic efficiency against cefotaxime and carbapenems.

DISCUSSION

As MBLs are increasingly spreading in Gram-negative bacteria, novel variants of known MBLs with altered substrate specificities will be discovered. Here, we have characterized VIM-52, a novel H224R VIM-1 variant present in a clinical isolate of *K. pneumoniae* belonging to ST147, both phenotypically and biochemically. The *bla*$_{VIM-52}$ gene
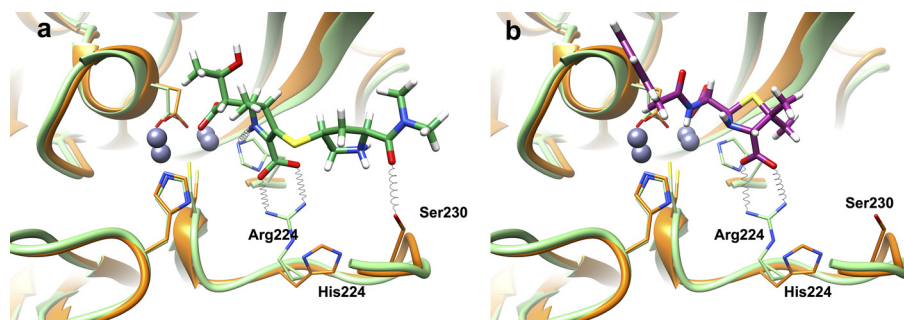

FIG 6 Molecular determinants for the selectivity of meropenem and benzylpenicillin on specific VIM variants. The docking complex of meropenem (a, dark green) and benzylpenicillin (b, magenta) with the R224/R228 variant of VIM (colored in light green) is superposed with the H224/S228 variant (colored in orange). The zinc ions are represented as mauve spheres and the hydrogen bonds as black strings.

TABLE 4 Steady-state kinetic parameters for the VIM-52 mutants S228D and S228R

Antibiotic(s)	VIM52-S228D					VIM52-S228R					
	k_{cat} (s^{-1})	K_m (μM)	k_{cat}/K_m (μM^{-1} s^{-1})	R4[a]	R5[b]	k_{cat} (s^{-1})	K_m (μM)	k_{cat}/K_m (μM^{-1} s^{-1})	R6[c]	R7[d]	R8[e]
Benzylpenicillin	840 ± 60	84 ± 4	10 ± 2	**3.9**	**294**	320 ± 20	16 ± 2	20 ± 4	**7.7**	**590**	**5**
Cephalothin	350 ± 50	30 ± 4	11 ± 3	**2**	**2**	500 ± 70	25 ± 3	20 ± 3	**3.6**	**4**	**1.8**
Ceftazidime	>20	>280	0.07 ± 0.01	**5.8**	**1**	>2.5	>550	0.005 ± 0.001	**0.4**	**0.06**	**11**
Cefepime	>30	>300	0.1 ± 0.01	**1**	**0.03**	>1.5	>320	0.005 ± 0.002	**0.05**	**0.001**	**0.05**
Cefotaxime	270 ± 10	65 ± 8	4 ± 0.6	**1.2**	**6**	450 ± 60	50 ± 5	9 ± 2	**2.7**	**13**	**1.6**
Imipenem	2.5 ± 0.4	0.3 ± 0.05	8 ± 2.5	**4.4**	**6**	20 ± 1	1 ± 0.2	20 ± 5	**11**	**15**	**11**
Meropenem	3 ± 0.2	1.5 ± 0.3	2 ± 0.5	**4.4**	**7.4**	0.2 ± 0.04	0.03 ± 0.01	6.6 ± 3	**15**	**25**	**2.7**
Ertapenem	1.8 ± 0.3	2.8 ± 0.4	0.6 ± 0.2	**1**	**ND**	0.6 ± 0.1	0.06 ± 0.01	10 ± 3	**16**	**ND**	**500**

[a]R4, ratio k_{cat}/K_m VIM-52 S228D to k_{cat}/K_m VIM-52. Boldface type indicates ratio values; ND, not done.
[b]R5, ratio k_{cat}/K_m VIM-52 S228D to k_{cat}/K_m VIM-1.
[c]R6, ratio k_{cat}/K_m VIM-52 S228R to k_{cat}/K_m VIM-52.
[d]R7, ratio k_{cat}/K_m VIM-52 S228R to k_{cat}/K_m VIM-1.
[e]R8, ratio k_{cat}/K_m VIM-52 S228R to k_{cat}/K_m VIM-2.

was embedded in a class I integron carried by a 50-kb IncR-IncF plasmid, whose sequence is highly similar to a plasmid sequence (accession number NZ_CP027047.1) found in a *K. pneumoniae* strain 1_GR_13, also belonging to ST147 (21) and isolated from a Greek patient in 2013. Thus, it is likely that the patient acquired *Kp*_20150593 during his hospital stay in Greece.

Constitutive expression of the *bla*$_{VIM-52}$ gene in *E. coli* strain TOP10 suggested that VIM-52 is a carbapenemase with impaired cefepime hydrolysis (MIC = 0.25 μg/ml) compared to VIM-1 (MIC = 64 μg/ml). Steady-state kinetic parameters confirmed the phenotypical observation and revealed VIM-52 to have a nearly 40-fold lower activity against cefepime compared to VIM-1. These results are in line with a recent publication that compared the MIC values of VIM-1 and VIM-52 (22). While this group observed that the H224R mutation had no or poor effect on the level of carbapenem resistance, they noticed a significant drop in MICs for ceftazidime (4-fold), similar to what we observed, but they did not test cefepime.

Amino acids at position 224 and 228 are known to be important for substrate binding (17). In order to further explore the amino acid specificities at these positions, we prepared several point mutant derivatives by directed mutagenesis. We were able to show that the presence of an arginine at position 228 affects the substrate profile, i.e., an increased catalytic efficiency against imipenem and meropenem and a decreased catalytic efficiency against cefepime and ceftazidime (Table 4). This is in agreement with the activity profile of VIM-13 and VIM-19, respectively (23, 24).

In many subclass B1 (5, 25) and B2 (12) MBLs, the conserved Lys residue at position 224, close to the active site, plays an important role in substrate binding (17). In the case of VIM enzymes, K224 is substituted by H224 in VIM-1 and by Y224 in VIM-2. The shorter side chain of histidine and the uncharged lateral chain of tyrosine prevent the interaction of these two amino acids with the carboxylate moiety (C4 or C3) of the substrate. The presence of K224 allows the interaction with the substrate but also creates a stronger interaction with α- carbonyl moiety of the main chain of A231 and the water molecule shared with H196. This mutation favors a better docking of the antibiotic in the active site pocket and the polarization of the water molecule may increase the acid Lewis strength of the Zn2 and its hydrolytic activity (26). On the other hand, the presence of K224 resulted in a decrease of the k_{cat} value and an increase of the K_m value for cefepime, which resulted in a sharp decrease of the catalytic efficiency compared to VIM-1 (R2 ratio for cefepime = 0.007) (Table 3). We noticed that the catalytic efficiency of this VIM-1 H224K mutant is enhanced for cefotaxime (R2 ratio for cefotaxime = 8). Knowing that the only difference between cefotaxime and cefepime structure is the nature of the C3 lateral chain, our hypothesis is that the presence of a bulky and positively charged C3 lateral chain of cefepime affects its positioning in the active site and therefore its hydrolysis by the MBL.

It has been hypothesized that R228 (17) may act as stabilizer of carbapenems in the catalytic pocket of the MBLs. This seems confirmed by the observation of the activity enhancement against carbapenems of the VIM-52 S228R (from 11- to 460-fold compared to VIM-52, VIM-1, or VIM-2). On the contrary, we confirmed that the substitution of S228 with arginine dramatically lowered the activity against ceftazidime and cefepime, while not against cefotaxime. Our data underline the importance of the large positively charged C3, especially when positions 224 and 228 are both positively charged (R). The presence of the lateral chain of arginine induced steric clashes and hindrance, compromising the hydrolysis of cefepime and ceftazidime.

Interestingly, with the mutation H224K VIM-1 (S228), we also observed an increased catalytic efficiency against imipenem and meropenem and a decreased catalytic efficiency against cefepime and ceftazidime as in S228R VIM-52. This further suggests that R228 could replace the K224 for substrate binding and confirmed the importance of residues 224 and 228 for the carbapenemase activity in MBL (13, 14, 25).

MATERIALS AND METHODS

Antibiotics. Kanamycin was purchased from MP Biomedicals, France. Chloramphenicol, benzylpenicillin, cephalotin, cefotaxime, and ceftazidime were purchased from Sigma-Aldrich, (Overijse, Belgium). Cefepime was a gift from Fresenius Kabi, (Schelle, Belgium). Imipenem and ertapenem were purchased from MSD, (Brussels, Belgium) and meropenem from AstraZeneca (Dilbeek, Belgium).

Bacterial isolates. The clinical strain $Kp\_20150593$ expressing the VIM-52-ß-lactamase was used for cloning of the bla_{VIM-52} gene. E. coli TOP10 (Invitrogen, Saint-Aubin, France) and Stellar E. coli competent cells (Invitrogen, Merelbeke, Belgium) were used for cloning, azide-resistant E. coli strain J53 for conjugation experiments, and E. coli strain Rosetta (DE3) (Novagen, Fontenay-sous-Bois, France) for overexpression experiments.

Bacterial identification, antimicrobial susceptibility testing, and carbapenemase detection. Bacterial identification to the species level was performed using matrix-assisted laser desorption–time of flight (MALDI-TOF) mass spectrometry (MALDI Biotyper; Bruker Daltonics, Bremen, Germany).

Antimicrobial susceptibility testing was determined by disc diffusion on Mueller-Hinton agar plates (Bio-Rad, Marnes-La-Coquette, France) according to the CLSI guidelines (CLSI M-100-S15). MIC values were determined by broth microdilution using Sensititre plates (Trek Diagnostic Systems, Cleveland, OH, USA).

Carbapenemase activity was assessed by biochemical (Rapidec, bioMérieux, Marcy-l-Etoile, France) and electrochemical BYG Carba tests (27). The carbapenemase gene was detected by an in-house PCR ISO15189 certified. PCR products were subsequently Sanger sequenced by an external sequencing provider (Macrogen, Seoul, Korea) (28).

Plasmid analysis, conjugation, and transformation assays. Plasmid DNA was extracted from isolate $Kp\_20150593$ by the Kieser method and analyzed by 0.7% agarose gel electrophoresis using as a plasmid size marker the plasmid extract of the E. coli NCTC50192 strain, which harbors four plasmids of 154, 66, 48, and 7 kb. The plasmid extract of $Kp\_20150593$ was used to transform E. coli TOP10 by electroporation using the Gene Pulser II apparatus. Transformants were selected on LB agar plates containing 100 μg/ml of ampicillin. A solid mating experiment was performed using E. coli J53 (azide resistant) as a recipient strain. The transconjugants were selected on LB agar plate containing 100 μg/ml of azide and 100 μg/ml of ampicillin. Transformants and transconjugants were tested by disk diffusion and broth microdilution antibiograms and colony PCR using primers targeting the bla_{VIM} gene (29).

Whole-genome sequencing. Genomic DNA was extracted using NucliSENS easyMag (bioMérieux, Marcy-l'Etoile, France), following the manufacturer's instructions. A dual-indexed Illumina sequencing library was constructed using Nextera DNA Flex library preparation (Illumina Inc, CA, USA). Libraries were pooled and 100 pM was sequenced on the Illumina iSeq100 (2 × 150 bp). Sequence quality was assessed by FastQC. Reads were trimmed using Trimmomatic. Genome assembly was performed using Spades and assembly quality was assessed using Quast. Resistance genes and replicons were identified using ResFinder (https://cge.cbs.dtu.dk/services/ResFinder/) and PlasmidFinder (https://cge.cbs.dtu.dk/services/PlasmidFinder/), respectively. The contig number 38, harboring the bla_{VIM-52} gene (accession number GenBank ANI25016.1), was annotated using RAST (https://rast.nmpdr.org/), Integrall (http://integrall.bio.ua.pt/), and ISFinder (https://isfinder.biotoul.fr/blast.php). The contig number 38 sequence was aligned against K. pneumoniae (TaxID 573) using the NCBI BLAST tool. Multilocus sequence type (MLST) was determined using BIGSdb-Kp Pasteur database, while capsular type was determined using Kaptive webtool (http://kaptive.holtlab.net/).

Site-directed mutagenesis, cloning, and expression. Bla_{VIM-1} and bla_{VIM-52} genes and their ribosome binding site (RBS) were amplified using Q5 High-Fidelity DNA polymerase (Bioké, Leiden, The Netherlands) and ligated into the pCR-Blunt II-TOPO vector according to the manufacturer's instructions (Thermo Fisher, Brussels, Belgium). Ligation products were used to transform E. coli TOP10 by electroporation and transformants were selected on LB containing 50 μg/ml kanamycin. Colonies were screened by PCR using M13 forward (−20) and M13 reverse universal primers. Amplified DNA were sequenced by an external DNA sequencing service (Macrogen Inc., Seoul, South Korea) using the same primers to check sequence and orientation of the inserted fragment.

These two plasmids, pTOPO-VIM-1 and pTOPO-VIM-52, were used for PCR site-directed mutagenesis using the QuikChange II site-directed mutagenesis kit according to the manufacturer's recommendations (Agilent Technologies, Diegem, Belgium) to obtain the following variants: VIM-1 H224A, H224D, and H224K; VIM-52 S228A, S228D, S228K, and S228R, after which they were ligated into the pCR-Blunt II-TOPO plasmid. The MIC values of all the *E. coli* TOP10 strains constitutively expressing VIM-1 and VIM-52 and their mutants were determined by broth microdilution as described above.

Protein production and purification. Bla_{VIM-1} and bla_{VIM-52} genes and their variants were amplified using Q5 High-Fidelity DNA polymerase and introduced into the pET26b plasmid using the In-Fusion HD cloning kit (TaKaRa bio, Saint-Germain-en-Laye, France), following the manufacturer's instructions. The In-Fusion reaction mixtures were used to transform Stellar *E. coli* competent cells and transformants were selected on LB containing 50 μg/ml kanamycin. Colonies were screened by PCR using T7 primers. All the enzymes were produced in *E. coli* Rosetta (DE3) carrying pET26b/bla_{VIM-52}, pET26b/bla_{VIM-1}, and mutants thereof. The cultures were performed in LB medium supplemented with kanamycin (50 μg/ml) and chloramphenicol (30 μg/ml). The cultures were incubated overnight at 37°C under agitation and 40 ml was used to inoculated 1 liter of fresh LB medium supplemented as described above. IPTG (isopropyl-β-D-thiogalactopyranoside; 50 μM final concentration) was added when the culture reached to an optical density at 600 nm (OD$_{600}$) of 0.7 and then the cultures were incubated overnight at 18°C. Cells were harvested by centrifugation (5,000 $\times$ *g* for 10 min at 4°C) and the pellets were resuspended in 40 ml of 50 mM MES buffer pH 6.5 with 50 μM ZnCl$_2$ (buffer A). The bacteria were disrupted with the help of a cell disrupter (Emulsiflex C3; Avestin GmbH, Germany), which allows cell lysis at a pressure of 5.500 kPa. The lysates were centrifuged at 45,000 $\times$ *g* for 30 min. The cleared supernatants were recovered and filtered through a 45-μm filter and were then loaded onto a Q Sepharose HP (GE Healthcare, Machelen, Belgium) equilibrated with buffer A. The enzymes were eluted with a salt gradient using buffer A and 50 mM MES, pH 6.5 with 1 M NaCl, (buffer B). The fractions containing β-lactamase activity were pooled, and then dialyzed overnight in 25 mM HEPES, pH 7.5, 50 μM ZnCl$_2$, 1.2 M (NH$_4$)$_2$SO$_4$. The dialysis sample was loaded onto Butyl Sepharose High Performance (20 ml) (Pharmacia Biotech) previously equilibrated with 25 mM HEPES, pH 7.5, 50 μM ZnCl$_2$, 1.2M (NH$_4$)$_2$SO$_4$ (buffer A). The enzymes were eluted with a salt-out gradient between buffer A and 25 mM HEPES, pH 7.5, 50 μM ZnCl$_2$ (buffer B). The active fractions were collected and concentrated on a YM-10 membrane (Amicon, Beverly, Mass.) to a final volume of 2 ml. The sample was loaded in a molecular sieve Superdex 75 GL (10/300) column (GE Healthcare, Belgium) equilibrated in 50 mM HEPES buffer pH 7.5, 50 μM ZnCl$_2$ containing 0.2 M NaCl. At the end of each purifications step, β-lactamase activity was routinely measured spectrophotometrically by following the hydrolysis of a solution of 100 μM imipenem as previously described (14).

Steady-state kinetic parameters (K_m and k_{cat}) were determined by measuring substrate hydrolysis under initial rate conditions and using the Hanes-Wolf linearization from the Michaelis-Menten equation (30). Kinetic experiments were performed by following the hydrolysis of each substrate at 30°C in 25 mM HEPES buffer pH 7.5, 50 μM ZnCl$_2$ .The data were collected with a Specord 50 PLUS spectrophotometer (Analytik, Jena, Germany). Each kinetic value is the mean of three different measurements.

Molecular modeling. Three-dimensional structures of mutants were generated using the swapaa command implemented in UCSF CHIMERA (31), starting from the structure of VIM-1 (PDB code 5N5I) (16).

Molecular dynamics simulations were performed with GROMACS version 4.6.5 (32) using the OPLS-AA force field (33). The protein was centered in a cubic periodic box with at least 1.0 nm on each side. The simulation box was then filled with TIP4P water molecules and the system neutralized with Na$^+$ and Cl$^-$ ions until reaching the physiological ionic strength (150 mM). Each system was energy-minimized until convergence using a steepest descents algorithm. Molecular dynamics with position restraints on backbone, with the exception of residues 223 to 232, which were unrestrained, was then performed for 50 ns. The Parrinello-Rahman method was used for pressure coupling (34) and the temperature was coupled using the Nosé-Hoover method at 300 K (35, 36). Electrostatics were calculated with the particle-mesh Ewald method (37). The P-LINCS algorithm (38) was used to constrain bond lengths and a time step of 2 fs was used throughout. All frames from each simulation were clustered and the most representative conformations were used as input for molecular docking (see below). HOP software version 0.4.0 alpha2 (https://github.com/Becksteinlab/hop) (39) was used for water molecule dynamics analysis. Molecular docking calculations were performed using the GOLD software (40) from the CCDC_2020 suite and the GoldScore scoring function, with the representative conformers from molecular dynamics simulations as receptors and the binding sites defined as a 20 Å radius around the Zn1 ion. All other parameters had default values.

SUPPLEMENTAL MATERIAL

Supplemental material is available online only.

SUPPLEMENTAL FILE 1, PDF file, 1.6 MB.

REFERENCES

1. Theuretzbacher U. 2017. Global antimicrobial resistance in Gram-negative pathogens and clinical need. Curr Opin Microbiol 39:106–112. https://doi.org/10.1016/j.mib.2017.10.028.

2. Boyd SE, Livermore DM, Hooper DC, Hope WW. 2020. Metallo-beta-lactamases: structure, function, epidemiology, treatment options, and the development pipeline. Antimicrob Agents Chemother 64:e00397-20. https://doi.org/10.1128/AAC.00397-20.

3. Sabath LD, Abraham EP. 1966. Zinc as a cofactor for cephalosporinase from Bacillus cereus 569. Biochem J 98:11C–13C. https://doi.org/10.1042/bj0980011c.

4. Hansen GT. 2021. Continuous evolution: perspective on the epidemiology of carbapenemase resistance among Enterobacterales and other Gram-negative bacteria. Infect Dis Ther 10:75–92. https://doi.org/10.1007/s40121-020-00395-2.

5. Mojica MF, Bonomo RA, Fast W. 2016. B1-metallo-beta-lactamases: where do we stand? Curr Drug Targets 17:1029–1050. https://doi.org/10.2174/1389450116666151001105622.

6. Lauretti L, Riccio ML, Mazzariol A, Cornaglia G, Amicosante G, Fontana R, Rossolini GM. 1999. Cloning and characterization of blaVIM, a new integron-borne metallo-beta-lactamase gene from a Pseudomonas aeruginosa clinical isolate. Antimicrob Agents Chemother 43:1584–1590. https://doi.org/10.1128/AAC.43.7.1584.

7. Yong D, Toleman MA, Giske CG, Cho HS, Sundman K, Lee K, Walsh TR. 2009. Characterization of a new metallo-beta-lactamase gene, bla(NDM-1), and a novel erythromycin esterase gene carried on a unique genetic structure in Klebsiella pneumoniae sequence type 14 from India. Antimicrob Agents Chemother 53:5046–5054. https://doi.org/10.1128/AAC.00774-09.

8. Naas T, Oueslati S, Bonnin RA, Dabos ML, Zavala A, Dortet L, Retailleau P, Iorga BI. 2017. Beta-lactamase database (BLDB)—structure and function. J Enzyme Inhib Med Chem 32:917–919. https://doi.org/10.1080/14756366.2017.1344235.

9. Oelschlaeger P, Ai N, Duprez KT, Welsh WJ, Toney JH. 2010. Evolving carbapenemases: can medicinal chemists advance one step ahead of the coming storm? J Med Chem 53:3013–3027. https://doi.org/10.1021/jm9012938.

10. Borgianni L, Vandenameele J, Matagne A, Bini L, Bonomo RA, Frere JM, Rossolini GM, Docquier JD. 2010. Mutational analysis of VIM-2 reveals an essential determinant for metallo-beta-lactamase stability and folding. Antimicrob Agents Chemother 54:3197–3204. https://doi.org/10.1128/AAC.01336-09.

11. Franceschini N, Caravelli B, Docquier JD, Galleni M, Frere JM, Amicosante G, Rossolini GM. 2000. Purification and biochemical characterization of the VIM-1 metallo-beta-lactamase. Antimicrob Agents Chemother 44:3003–3007. https://doi.org/10.1128/AAC.44.11.3003-3007.2000.

12. Garau G, Garcia-Saez I, Bebrone C, Anne C, Mercuri P, Galleni M, Frere JM, Dideberg O. 2004. Update of the standard numbering scheme for class B beta-lactamases. Antimicrob Agents Chemother 48:2347–2349. https://doi.org/10.1128/AAC.48.7.2347-2349.2004.

13. Garcia-Saez I, Docquier JD, Rossolini GM, Dideberg O. 2008. The three-dimensional structure of VIM-2, a Zn-beta-lactamase from Pseudomonas aeruginosa in its reduced and oxidised form. J Mol Biol 375:604–611. https://doi.org/10.1016/j.jmb.2007.11.012.

14. Lassaux P, Traore DA, Loisel E, Favier A, Docquier JD, Sohier JS, Laurent C, Bebrone C, Frere JM, Ferrer JL, Galleni M. 2011. Biochemical and structural characterization of the subclass B1 metallo-beta-lactamase VIM-4. Antimicrob Agents Chemother 55:1248–1255. https://doi.org/10.1128/AAC.01486-09.

15. Leiros HK, Edvardsen KS, Bjerga GE, Samuelsen O. 2015. Structural and biochemical characterization of VIM-26 shows that Leu224 has implications for the substrate specificity of VIM metallo-beta-lactamases. FEBS J 282:1031–1042. https://doi.org/10.1111/febs.13200.

16. Salimraj R, Hinchliffe P, Kosmopoulou M, Tyrrell JM, Brem J, van Berkel SS, Verma A, Owens RJ, McDonough MA, Walsh TR, Schofield CJ, Spencer J. 2019. Crystal structures of VIM-1 complexes explain active site heterogeneity in VIM-class metallo-beta-lactamases. FEBS J 286:169–183. https://doi.org/10.1111/febs.14695.

17. Mojica MF, Mahler SG, Bethel CR, Taracila MA, Kosmopoulou M, Papp-Wallace KM, Llarrull LI, Wilson BM, Marshall SH, Wallace CJ, Villegas MV, Harris ME, Vila AJ, Spencer J, Bonomo RA. 2015. Exploring the role of residue 228 in substrate and inhibitor recognition by VIM metallo-beta-lactamases. Biochemistry 54:3183–3196. https://doi.org/10.1021/acs.biochem.5b00106.

18. Karampatakis T, Antachopoulos C, Iosifidis E, Tsakris A, Roilides E. 2016. Molecular epidemiology of carbapenem-resistant Klebsiella pneumoniae in Greece. Future Microbiol 11:809–823. https://doi.org/10.2217/fmb-2016-0042.

19. Ludden C, Lotsch F, Alm E, Kumar N, Johansson K, Albiger B, Huang TD, Denis O, Hammerum AM, Hasman H, Jalava J, Raisanen K, Dortet L, Jousset AB, Gatermann S, Haller S, Cormican M, Brennan W, Del Grosso M, Monaco M, Schouls L, Samuelsen O, Pirs M, Cerar T, Oteo-Iglesias J, Perez-Vazquez M, Sjostrom K, Edquist P, Hopkins KL, Struelens MJ, Palm D, Monnet DL, Kohlenberg A. 2020. Cross-border spread of bla NDM-1- and bla OXA-48-positive Klebsiella pneumoniae: a European collaborative analysis of whole genome sequencing and epidemiological data, 2014 to 2019. Euro Surveill 25:2000627. https://doi.org/10.2807/1560-7917.ES.2020.25.20.2000627.

20. Peirano G, Chen L, Kreiswirth BN, Pitout JDD. 2020. Emerging antimicrobial-resistant high-risk Klebsiella pneumoniae clones ST307 and ST147. Antimicrob Agents Chemother 64:e01148-20. https://doi.org/10.1128/AAC.01148-20.

21. Pitt ME, Elliott AG, Cao MD, Ganesamoorthy D, Karaiskos I, Giamarellou H, Abboud CS, Blaskovich MAT, Cooper MA, Coin LJM. 2018. Multifactorial chromosomal variants regulate polymyxin resistance in extensively drug-resistant Klebsiella pneumoniae. Microb Genom 4:e000158. https://doi.org/10.1099/mgen.0.000158.

22. Cheng Z, Shurina BA, Bethel CR, Thomas PW, Marshall SH, Thomas CA, Yang K, Kimble RL, Montgomery JS, Orischak MG, Miller CM, Tennenbaum JL, Nix JC, Tierney DL, Fast W, Bonomo RA, Page RC, Crowder MW. 2019. A single salt bridge in VIM-20 increases protein stability and antibiotic resistance under low-zinc conditions. mBio 10:e02412-19. https://doi.org/10.1128/mBio.02412-19.

23. Merino M, Perez-Llarena FJ, Kerff F, Poza M, Mallo S, Rumbo-Feal S, Beceiro A, Juan C, Oliver A, Bou G. 2010. Role of changes in the L3 loop of the active site in the evolution of enzymatic activity of VIM-type metallo-beta-lactamases. J Antimicrob Chemother 65:1950–1954. https://doi.org/10.1093/jac/dkq259.

24. Rodriguez-Martinez JM, Nordmann P, Fortineau N, Poirel L. 2010. VIM-19, a metallo-beta-lactamase with increased carbapenemase activity from Escherichia coli and Klebsiella pneumoniae. Antimicrob Agents Chemother 54:471–476. https://doi.org/10.1128/AAC.00458-09.

25. Docquier JD, Lamotte-Brasseur J, Galleni M, Amicosante G, Frere JM, Rossolini GM. 2003. On functional and structural heterogeneity of VIM-type metallo-beta-lactamases. J Antimicrob Chemother 51:257–266. https://doi.org/10.1093/jac/dkg067.

26. Yamaguchi Y, Jin W, Matsunaga K, Ikemizu S, Yamagata Y, Wachino J, Shibata N, Arakawa Y, Kurosaki H. 2007. Crystallographic investigation of the inhibition mode of a VIM-2 metallo-beta-lactamase from Pseudomonas aeruginosa by a mercaptocarboxylate inhibitor. J Med Chem 50:6647–6653. https://doi.org/10.1021/jm701031n.

27. Bogaerts P, Yunus S, Massart M, Huang TD, Glupczynski Y. 2016. Evaluation of the BYG Carba test, a new electrochemical assay for rapid laboratory detection of carbapenemase-producing Enterobacteriaceae. J Clin Microbiol 54:349–358. https://doi.org/10.1128/JCM.02404-15.

28. Bogaerts P, Rezende de Castro R, de Mendonca R, Huang TD, Denis O, Glupczynski Y. 2013. Validation of carbapenemase and extended-spectrum beta-lactamase multiplex endpoint PCR assays according to ISO 15189. J Antimicrob Chemother 68:1576–1582. https://doi.org/10.1093/jac/dkt065.

29. Bogaerts P, Huang TD, Rodriguez-Villalobos H, Bauraing C, Deplano A, Struelens MJ, Glupczynski Y. 2008. Nosocomial infections caused by multidrug-resistant Pseudomonas putida isolates producing VIM-2 and VIM-4 metallo-beta-lactamases. J Antimicrob Chemother 61:749–751. https://doi.org/10.1093/jac/dkm529.

30. Cornish-Bowden A. 1995. Fundamentals of enzyme kinetics. Portland Press, London, United Kingdom.

31. Pettersen EF, Goddard TD, Huang CC, Couch GS, Greenblatt DM, Meng EC, Ferrin TE. 2004. UCSF Chimera—a visualization system for exploratory research and analysis. J Comput Chem 25:1605–1612. https://doi.org/10.1002/jcc.20084.

32. Pronk S, Pall S, Schulz R, Larsson P, Bjelkmar P, Apostolov R, Shirts MR, Smith JC, Kasson PM, van der Spoel D, Hess B, Lindahl E. 2013. GROMACS 4.5: a high-throughput and highly parallel open source molecular simulation toolkit. Bioinformatics 29:845–854. https://doi.org/10.1093/bioinformatics/btt055.

33. Kaminski GA, Friesner RA, Tirado-Rives J, Jorgensen WL. 2001. Evaluation and reparametrization of the OPLS-AA force field for proteins via comparison with accurate quantum chemical calculations on peptides. J Phys Chem B 105:6474–6487. https://doi.org/10.1021/jp003919d.

34. Parrinello M, Rahman A. 1981. Polymorphic transitions in single crystals: a new molecular dynamics method. J Appl Phys 52:7182–7190. https://doi.org/10.1063/1.328693.

35. Hoover WG. 1985. Canonical dynamics: equilibrium phase-space distributions. Phys Rev A Gen Phys 31:1695–1697. https://doi.org/10.1103/physreva.31.1695.

36. Nosé S. 1984. A unified formulation of the constant temperature molecular dynamics methods. J Chem Phys 81:511–519. https://doi.org/10.1063/1.447334.

37. Essmann U, Perera L, Berkowitz ML, Darden T, Lee H, Pedersen LG. 1995. A smooth particle mesh Ewald method. J Chem Phys 103:8577–8593. https://doi.org/10.1063/1.470117.

38. Hess B. 2008. P-LINCS: a parallel linear constraint solver for molecular simulation. J Chem Theory Comput 4:116–122. https://doi.org/10.1021/ct700200b.

39. Beckstein O, Michaud-Agrawal N, Woolf TB. 2009. Quantitative analysis of water dynamics in and near proteins. Biophys J 96:601a. https://doi.org/10.1016/j.bpj.2008.12.3147.

40. Verdonk ML, Cole JC, Hartshorn MJ, Murray CW, Taylor RD. 2003. Improved protein-ligand docking using GOLD. Proteins 52:609–623. https://doi.org/10.1002/prot.10465.